water

MDPI

Article

Analysis of Climate-Related Risks for Chile's Coastal Settlements in the ARClim Web Platform

Patricio Winckler [1,2,3,*], Manuel Contreras-López [4], René Garreaud [5,6], Francisco Meza [7,8], Cristián Larraguibel [9], César Esparza [10], Stefan Gelcich [11,12], Mark Falvey [13] and Javiera Mora [14]

1 Escuela de Ingeniería Civil Oceánica, Universidad de Valparaíso, Av. Brasil 1786, Valparaíso 2362844, Chile
2 National Research Center for Integrated Natural Disaster Management (CIGIDEN), Vicuña Mackenna 4860, Macul 7820436, Chile
3 Centro de Observación Marino para Estudios de Riesgos del Ambiente Costero (COSTAR), Universidad de Valparaíso, Av. Brasil 1786, Valparaíso 2362844, Chile
4 Independent Researcher, Uruguay 556, of.304, Valparaíso 2340145, Chile
5 Department of Geophysics, Universidad de Chile, Av. Blanco Encalada 2002, Santiago 8370449, Chile
6 Center for Climate and Resilience Research (CR2), Universidad de Chile, Av. Blanco Encalada 2002, Santiago 8370449, Chile
7 Facultad de Agronomía e Ingeniería Forestal, Pontificia Universidad Católica de Chile, Vicuña Mackenna 4860, Macul 7820436, Chile
8 Centro de Cambio Global UC, Pontificia Universidad Católica de Chile, Avda. Libertador Bernardo O'Higgins 340, Santiago 8331150, Chile
9 Instituto de Geografía, Pontificia Universidad Católica de Valparaíso, Avenida Brasil 2241, Valparaíso 2362807, Chile
10 Departamento de Ingeniería Hidráulica y Ambiental, Pontificia Universidad Católica de Chile, Vicuña Mackenna 4860, Macul 7820436, Chile
11 Instituto Milenio en Socio-Ecología Costera, Facultad de Ciencias Biológicas, Pontificia Universidad Católica de Chile, Avda. Libertador Bernardo O'Higgins 340, Santiago 8331150, Chile
12 Center of Applied Ecology and Sustainability, Pontificia Universidad Católica de Chile, Avda. Libertador Bernardo O'Higgins 340, Santiago 8331150, Chile
13 Meteodata Limitada, Domeyko 1864, Santiago 8370377, Chile
14 Independent Researcher, El Solar 318, Maipu 9251990, Chile
* Correspondence: patricio.winckler@uv.cl; Tel.: +56-9-42572974

Abstract: The web-based tool ARClim provides an atlas of climate change-related risk assessments spanning over 50 environmental and productive sectors in Chile. This paper illustrates the implementation of ARClim on two coastal sectors, operational downtime in fishing coves and flooding in coastal settlements, aiming to provide a tool to visualize comparative estimates of risk, which may enable decision makers and stakeholders to prioritize adaptation measures. The risk is calculated as a function of the hazard, exposure, and sensitivity. Exposure and sensitivity are characterized using present day information. To assess the hazard, wave climate for a historical period (1985–2004) and a projection (2026–2045) were modeled with six general circulation models (GCMs) for an RCP8.5 scenario. Similarly, sea-level rise was computed from 21 GCMs. Results show that the flooding hazard is mostly dependent on sea-level rise, with waves playing a minor role. However, the flooding risk is highly variable along the coast, due to differences in the exposure, which strongly depends on the population of each settlement. The analysis of increased operational downtime in fishing coves also shows risk, which is dependent of the size of each site. Lastly, limitations of the analysis and opportunities for improvement are discussed.

Keywords: fishing coves; coastal flooding; climate change; coastal flooding; operational downtime

check for updates

Citation: Winckler, P.; Contreras-López, M.; Garreaud, R.; Meza, F.; Larraguibel, C.; Esparza, C.; Gelcich, S.; Falvey, M.; Mora, J. Analysis of Climate-Related Risks for Chile's Coastal Settlements in the ARClim Web Platform. *Water* **2022**, *14*, 3594. https://doi.org/10.3390/w14223594

Academic Editors: Marcel J. F. Stive, José A. Jiménez and Yongping Chen

Received: 31 August 2022
Accepted: 24 October 2022
Published: 8 November 2022

1. Introduction

On 13 June 2022, a new Framework Law on Climate Change (Law 21,455) was enacted in Chile [1]. Among several objectives, including the achievement of greenhouse gas

emission neutrality no later than 2050, the law requires the implementation of a sectoral plan for climate change adaptation in the coastal zone (Article 9°). Additionally, the law establishes the creation of a national information system on climate change (Title V) based on climate projections and vulnerability maps for the country. In this context, in 2020, the Ministry of the Environment launched the "Climate Change Risk Atlas for Chile" (ARClim), a platform aimed at providing a comprehensive analysis of climate-related risks at a national scale (https://arclim.mma.gob.cl/, accessed on 12 October 2022). Its overall objective is to provide relevant information for the design of policies and the implementation of adaptation measures [2]. The available risk assessments (52 at present) cover 12 social, environmental, and productive sectors.

ARCLIM was envisioned to communicate the main components of risk, namely, hazard, exposure, and vulnerability, using a common framework across many different socio-economic sectors of systems to facilitate comparison and analysis. Vulnerability is defined as a combination of sensitivity and adaptive capacity [3], where sensitivity is the degree to which a system is affected, either adversely or beneficially, by climate-related stimuli, and the adaptative capacity is the ability of a system to adjust to climate change to moderate potential damages, to take advantage of opportunities, or to cope with the consequences [4]. However, only few sectors considered in the web-based tool had developed a conceptual framework to account for adaptive capacity in a (semi)quantitative manner. On the contrary, sensitivity data were frequently available or relatively easy to develop. Under these conditions, the lead PI of the project decided for consistency to represent the vulnerability within the ARCLIM project focusing on the sensitivity component. Therefore, the risk was estimated from a combination (often multiplicative) of the exposure, sensitivity, and the hazard resulting from changes in climatic conditions affecting each sector. The basic methodology follows the definition of risk established by the Intergovernmental Panel on Climate Change [5], whose difference from previous approaches was described in [3]. Exposure gauges the presence of people, livelihoods, species or ecosystems, environmental functions, services and resources, and infrastructure that could be adversely affected by climate change. Sensitivity corresponds to the tendency to be adversely affected, including multiple physical, environmental, and social elements. Both exposure and sensitivity were evaluated in the present condition, while the hazard was computed as the difference between a near future and a historical period under a pessimistic greenhouse gas emissions scenario (RCP8.5). The use of RCP 8.5 was considered as the worst-case scenario according to the best available information (i.e., CMIP5) we had at hand when developing ARClim. The overall set of risk analyses was developed by 93 experts from 31 research centers and universities, in permanent coordination with the Ministry of Environment. The ARClim web platform (presently available in Spanish only), was built upon information delivered by these working groups and provides access to digital risk maps along with links to the underlying data and documentation.

For most of continental Chile, model-based climate change projections consistently indicate a continuation of an ongoing drying and warming, increasing the threat of intense, protracted droughts, and the number of heat waves [6]. Furthermore, the Chilean coastline is prone to climate-driven oceanographic hazards [7], the focus of this work. The country is characterized by strong latitudinal climatic gradients, ranging from one of the world's most arid regions in the extreme north (~18° S), to the cold tundra of Patagonia (~55° S). Its coastal geomorphology and high seismicity are shaped by the subduction of the Nazca Plate beneath the South American Plate, which together form the Peru–Chile trench. Between 18.4° S and 41.5° S, an almost linear coastline embraces major coastal cities and smaller settlements where artisanal fishing is one of the most important economic activities. To the south (41.5° S–55.6° S), the Chilean Inland Sea of Patagonia represents one the most extensive fjord regions in the world. These characteristics make Chile a natural laboratory to investigate climate trends and coastal hazards [7]. Specifically, climate-driven changes in mean sea-level rise and storminess are expected to affect the dynamics of coastal systems such as wetlands, estuaries, deltas, and dune fields. For urban areas, the impacts include

overtopping of lowlands, beach and cliff erosion, structural damage to coastal defenses, breakwaters, and promenades [8], operational downtime in commercial and fishing ports, saline intrusion into aquifers, and impacts on areas with cultural heritage. Here, we describe the development of risk assessments for two coastal systems and illustrate their application in ARClim, namely, the risk of flooding in coastal settlements and changes in operational downtime in artisanal fishing coves.

1.1. Coastal Flooding at Settlements

Several regional impact assessments of flooding under future climate have been developed, for example, in Great Britain [9,10], California [11], and Spain [12]. However, little such information is available for the western coast of South America, and is mostly contained in a few studies describing the impacts of recent storms in Chile [13,14]. The need for comprehensive climate risk assessments is particularly urgent, as nearly one million inhabitants, 5.7% of Chile's 17.6 million, dwell in low-elevation coastal zones (LECZs) below 10 m above mean sea level (masl). The nation's population in LECZ is lower than the global and Latin American averages of 10% and 6%, respectively [15], and is distributed across 433 coastal settlements in 100 municipalities. The scarce evidence of expected climate-driven impacts calls for action. For example, the authors of [16] showed that climate change could cause a slight increase in overtopping of coastal defenses by 2026–2045 and drastically increase its magnitude by 2081–2100, mainly driven by sea-level rise and, to a lesser degree, by storminess. This phenomenon will be accompanied by flooding of low-lying areas along Chile's 106,544 km of coastline. In this study, risk is analyzed as the impact associated with flooding of 433 coastal settlements due to a combination of waves, tides, storm surge, and sea-level rise.

1.2. Operational Downtime at Fishing Coves

By 2019, there were 24,806 women and 114,764 men registered as artisanal fishers countrywide, with landings of around 1.5 million tons from 545 fishing coves [17]. Artisanal fishing includes a variety of extractive activities including diving, gathering, and fishing. These activities are carried out either from the shore or using boats up to 18 m in length. Due to its coastal geomorphology, a large proportion of the coves are open to the Pacific Ocean and, thus, exposed to ocean swells. Most sheltered coves are in Patagonia (south of 41.6° S), where they are found within dense archipelagos or fjords. During coastal storms [18], artisanal fishing must be suspended to ensure the safety of vessels and fishers. The periods in which the extractive activity does not take place due to weather conditions (i.e., operational downtime) could represent losses in landings with consequent losses in fishers' income.

Few local assessments have studied the fundamental causes triggering coastal fishing infrastructure and port shutdowns along the Chilean coasts. The authors of [19], for example, conducted a 17 month long historical analysis of variables causing operational shutdowns in the fishing port of Hanga Piko, in Rapa Nui (Easter Island) concluding that extreme sea levels were mainly driven by wave setup, with lesser contribution of barometric setup and wind setup. As for projections of downtime, the authors of [20] concluded, using overtopping flow as a proxy, that downtime would increase for end-of-century projections (2070–2100) in the RCP8.5 scenario. Conversely, the authors of [21] combined several oceanographic and atmospheric drivers with vulnerability to compute the risk of operations for end of-century RCP8.5 scenarios; however, their scope is global and provides limited information for the coast of Chile. Lastly, the authors of [16] evaluated climate-driven impacts in seven Chilean ports under the RCP 8.5 scenario, concluding that downtime would increase in some ports and decrease in others for mid-century projections.

In this study, we aim to bridge the existing knowledge gap for the artisanal fishing sector by analyzing the risk associated with the loss of landings from fishing coves due to coastal storms.

2. Materials and Methods

ARClim was built upon a common conceptual framework considering normalized measures of hazard, exposure, sensitivity, and risk. This approach allows the comparison and eventual combination of different social, environmental, and productive sectors included in the web-based tool.

2.1. Projections of Changes in Wave Climate, Mean Sea Level, Storm Surge, and Tide

Data of wave climate, mean sea level, storm surge, and tide were used to compute the climate hazard in both systems under scrutiny. Wave climate, in combination with operational thresholds informed by fishers, was assumed to be the determinant variable for downtime at fishing coves. The flooding risk at coastal settlements, on the other hand, was computed as a combination of waves, sea-level rise, and other phenomena. The methodology to obtain wave climate and mean sea level is presented in the sections below. Due to the limited availability of oceanographic variables (e.g., wind fields used to force wave models), the projection was assessed for the period 2026–2045, while the historical period was set to 1985–2004.

2.1.1. Wave Climate

The wave climate for both periods was computed from a combination of a Pacific-wide model (135° E–65° W and 75° S–60° N) and the transformation of wave spectra to each study site. The wave model, WAVEWATCH III v4.18 [22], was forced by three-hourly wind data and daily ice coverage from six general circulation models (GCMs) available from the Coupled Model Intercomparison Project 5 [23,24]. Four GCMs (ACCESS 1.0, HadGEM2-ES, MIROC5, and MRI-CGM3) were selected on the basis of their ability to correctly reproduce the observed wave climate of the southeast Pacific Ocean [25], while two additional GCMs (EC-EARTH and CMCC) were included due to their high resolution in the Pacific Ocean. The ocean bottom was modeled with a spatial resolution of 1° using ETOPO2v2′s bathymetric data [26] in combination with a coastline from the GHHSGVIII database [27]. This parametrization showed a satisfactory performance offshore Chile [28].

Transformation of wave spectra from deep waters to representative nodes at a depth of 20 m at each study site was conducted for periods using Snell's law and small-amplitude wave theory, considering the effects of shoaling and refraction. Time series of significant wave height (H_s), period (T_m), and direction (θ_m) were then computed at each site. To correct systematic errors (biases) of each GCM in the historical period, a bias correction method based on the empirical Gumbel quantile mapping (EGQM) [29] was applied to the exceedance probability curves of significant wave height. To do this, wave fields forced by winds from the CFSR reanalysis [30] were taken as reference data to correct significant wave heights, as they provide the best available estimation of the wave climate off the Chilean coasts [28]. The computed biases for each GCM were applied to the projection, assuming that the statistical properties of the climate biases are maintained in the future [29]. With this procedure, time series of wave parameters (significant wave height H_s, mean period T_m and mean direction θ_m) were obtained in the vicinity of each fishing cove and coastal settlement.

Figure 1 shows the conceptual model to compute changes in wave climate within the projection (2026–2045) with respect to the historical period (1985–2004).

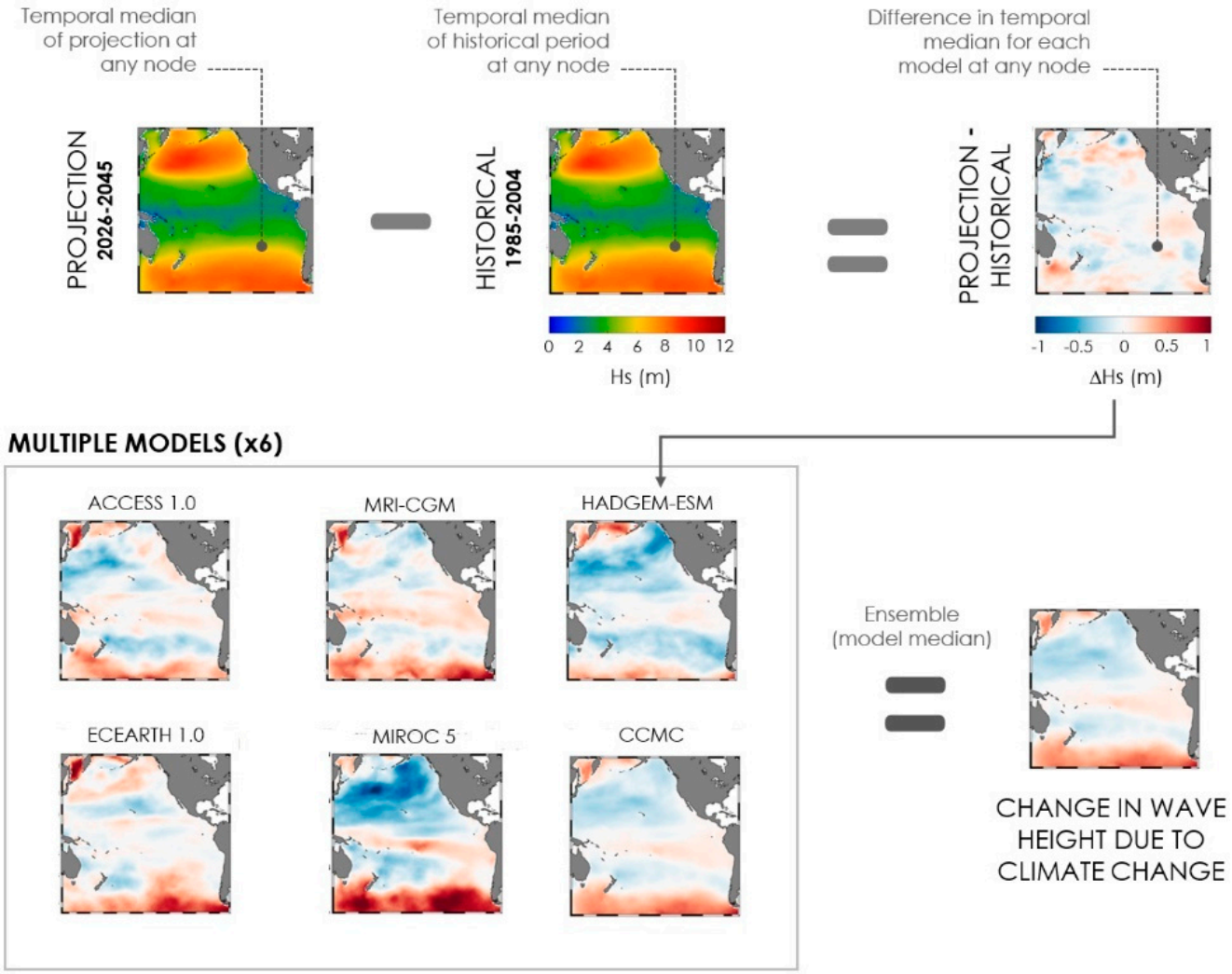

Figure 1. Conceptual model to compute changes in wave climate between the projection (2026–2045) with respect to the historical period (1985–2004). The top panel shows the computation of the temporal median for the historical period and projection and the difference between them in the modeling domain for one GCM (HADGEM-ESM as an example). The bottom panel shows the differences for all six models from which the median difference is computed and attributed to climate change. In this example, fields of significant wave heights are shown in the Pacific Ocean.

2.1.2. Sea-Level Rise

This study makes use of the projections of regional mean sea-level rise (*SLR*) rise that were presented in IPCC AR5 from CMIP5 [23,24]. The 1° × 1° resolution database is available from Hamburg University's Integrated Climate Data Center [31] for 21 GCMs under the RCP 8.5 scenario between 2007 and 2100 relative to the baseline period 1986–2005 (only the values corresponding to the period 2026–2045 were used in this study). These projections include estimates of the impact on sea level on (1) global thermal expansion and atmospheric loading, (2) ice sheet mass changes from surface mass balance, (3) ice sheet mass changes from ice dynamics, (4) glacier mass changes, (5) changes in land water from ground water extraction and reservoir impoundment, and (6) glacial isostatic adjustment due to the response of the solid Earth, the gravitational field, and the oceans to the growth and decay of the global ice sheets. Detailed calculation methods of each of these components can be consulted in [32]. The projection of *SLR* at Chilean coasts was computed from the ensemble mean of all 21 GCM regional projections in the entire Pacific basin. The GCMs were interpolated to each study site.

2.1.3. Storm Surge

Storm surge was based on data from [33] (Figure 65). Readily available data from 2010 were used as representative of the historical period, while data from 2040 were used for the projection. These data were interpolated to each site. The reason to use data which did not coincide with the analyzed periods was based on the practical reason that generating new data would have taken time and resources largely exceeding those allotted to the project.

2.1.4. Astronomical Tide

The maximum yearly astronomical tide (T) was obtained from tidal charts [34] and assumed to be invariant between both periods.

2.2. Flooding Risk of Coastal Settlements

An inventory of 433 coastal settlements was built from the information described in [35]. The risk analysis, however, was restricted to 256 coastal settlements whose coasts are open to swells from the Pacific Ocean, specifically from the northernmost Villa Frontera (18.339° S–70.333° W), to the southernmost Carelmapu (41.761° S–73.615° W), thus covering nearly 2600 km of Chilean coastline. The analysis excluded 177 sites located in the Chilean Inland Sea (41.5° S–55.6° S), as they are protected from ocean swells and do not experience a significant flooding hazard. However, exposure and sensitivity indices for these sites were included in ARClim database as they may still provide valuable information to decision makers. The computation of the hazard, exposure, sensitivity, and risk is presented below.

2.2.1. Hazard

We computed the historical flood level with respect to the lowest astronomical tide (Z_h) for the historical period (1985–2004), considering the contribution of wave runup (W_h), storm surge (S_h), and the maximum yearly astronomical tide (T).

$$Z_h = W_h + S_h + T, \tag{1}$$

where W_h was computed using Stockdon's formula [36], and time series of wave parameters (H_s, T_m, and θ_m) for each GCM were obtained in the vicinity of each coastal settlement. The mid-century projection (2026–2045) of the flood level (Z_p) included the projected wave runup (W_p), projected storm surge (S_p), the tide, and the sea-level rise between both periods (SLR).

$$Z_p = W_p + S_p + T + SLR. \tag{2}$$

From the time series of historical and projected flood levels, temporal medians for 20 years were computed for each GCM for both periods and their difference attributed to climate change. Figure 2 depicts the conceptual model used to define the flood level for the historical period and the projection.

The hazard index $\left(H^F\right)$ was then computed as the ratio of flooding level at each site and the maximum flooding level countrywide, $\max\{Z_p\}$, both computed for the projection,

$$H^F = Z_p / \max\{Z_p\}, \qquad 0 < H^F \leq 1. \tag{3}$$

with $\max\{Z_p\} = 3.76$ m corresponding to Astillero Bajo (41,761° S–73,615° W). Additionally, the historical and projected flooding, calculated using Equations (1) and (2), was used to compute the number of inhabitants and houses that were not flooded for the historical period but would be in the projection (i.e., those units whose height was between Z_h and Z_p), as an example of possible applications for which this database could be useful.

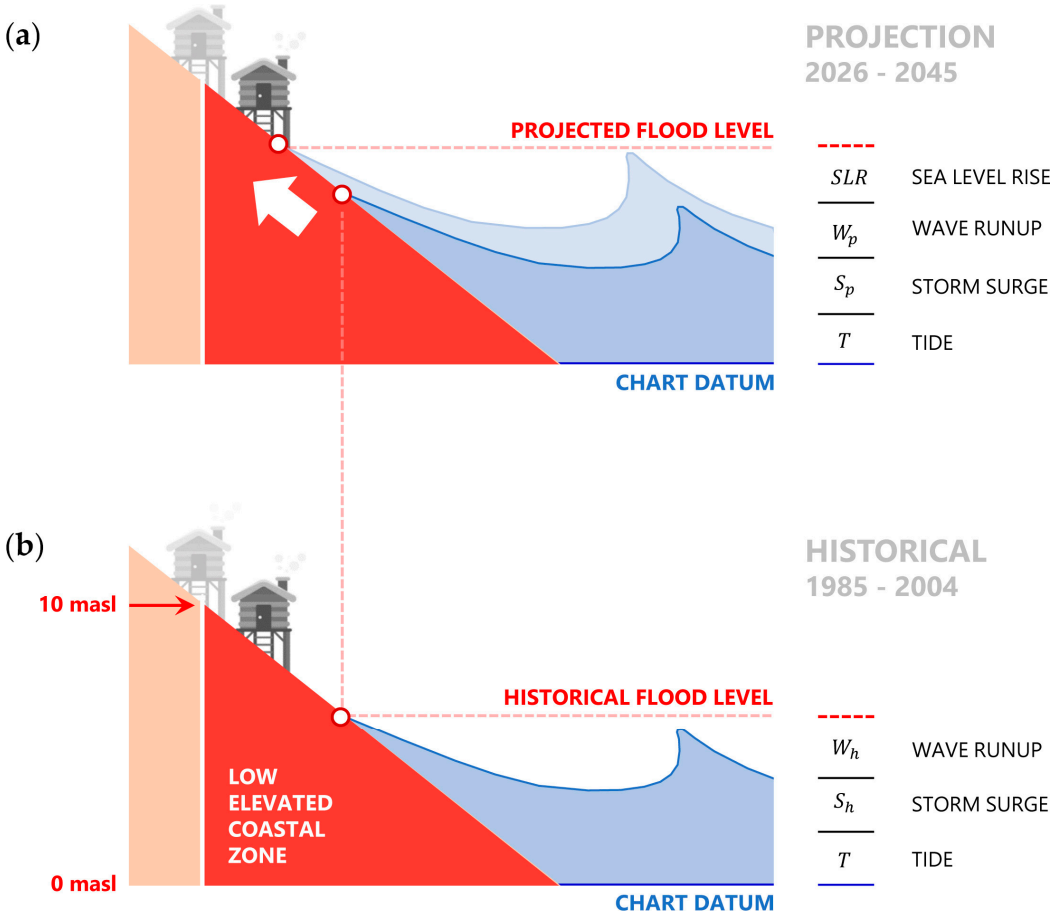

Figure 2. Conceptual model for the exposure and flood hazard used to compute the risk in coastal settlements. (**a**) Projected flood level (2026–2045) with respect to the historical chart datum used as a reference level. (**b**) historical flood level (1985–2004). The red arrow shows the upper bound of the low elevated coastal zone.

2.2.2. Exposure

The area below 10 masl, where population and housing were identified and used to compute the exposure, was obtained for each settlement from a digital elevation model built from satellite data (ALOS PALSAR, ALOS W3D, and ASTER GDEM-2) and 52 topographic surveys provided by SHOA, the Chilean Navy's hydrographic agency. Where only satellite data were available, the exposed area was conservatively computed considering pixels where at least one of the datasets showed an elevation below 10 masl. The cloud of pixels was then turned into a polygon by using a smooth line enclosing all the selected pixels. Figure 3a,b show an example of this process for Coquimbo Bay (29.959° S–71.334° W).

As satellite data showed poor performance in urban areas, the DEMs and the corresponding definition of the 10 masl were built solely from topographic surveys listed in Table 15 of [35] whenever available. These surveys, however, partially or totally covered a few sites under scrutiny. Details of this procedure are shown in [35] (Table 20). As an example, Figure 3c shows the polygon of exposed area generated from the topographic survey at Coquimbo Bay.

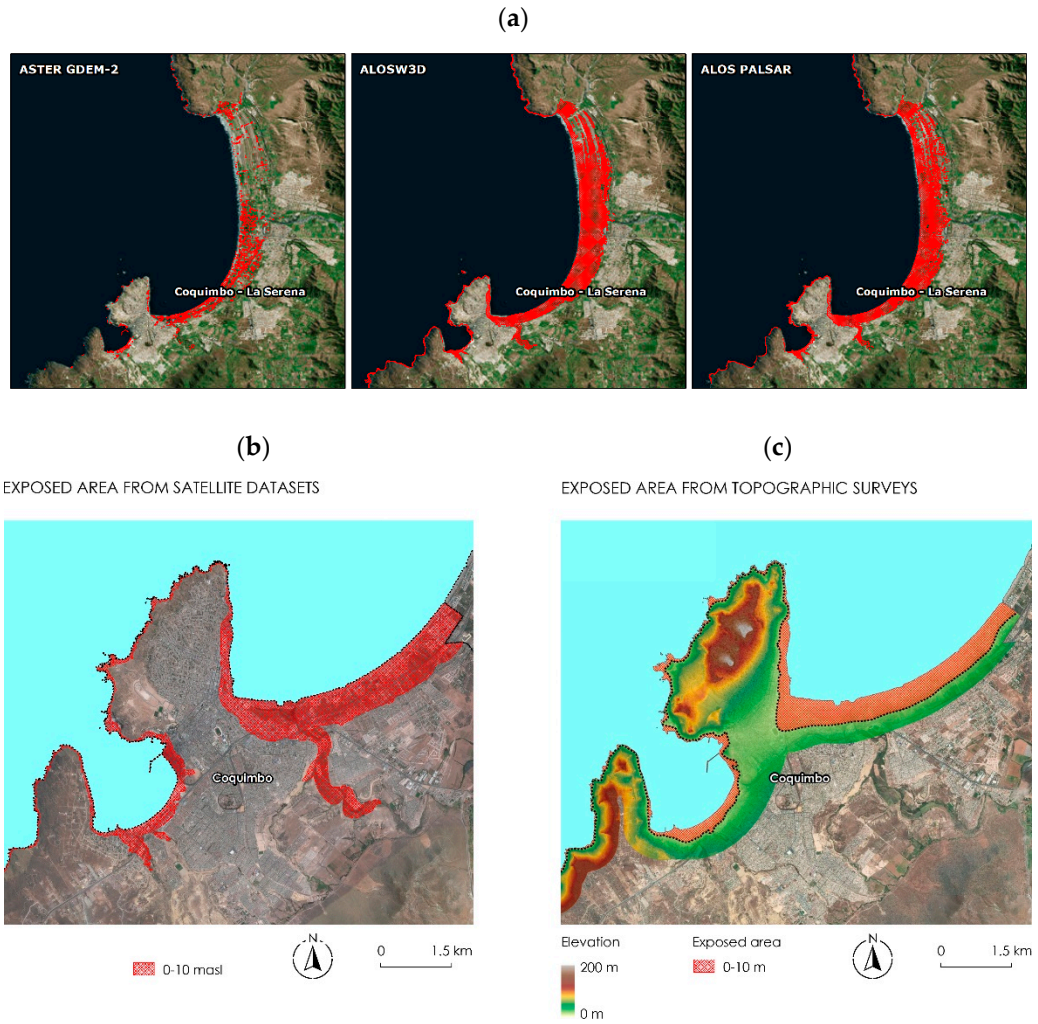

Figure 3. (**a**) Selection of pixels below masl from the three satellite datasets at Coquimbo Bay (29.959° S–71.334° W). (**b**) Polygon of exposed area generated from satellite data. (**c**) Polygon of exposed area generated from topographic surveys.

Once the exposure area data were available, an inventory of coastal settlements was built. Each settlement was identified by its name, latitude, longitude, municipality, region, category (city, town, village, or hamlet), type (urban or rural), and population and number of houses, obtained from the 2017 Census [37]. The inventory was used to compute the exposure and the sensitivity to flooding hazard due to a combination of waves, tides, storm surge, and sea-level rise. Table 1 summarizes the definition of each term and its value for the city of Arica, as an example. The complete inventory is available in the ARClim web platform, as described in the table caption.

The exposure (E^{FL}) was defined as the number of inhabitants per coastal settlement, normalized by the largest population of the analyzed sites. Numerically, exposure is restricted to $0 < E^{FL} \leq 1$, where $E^{FL} = 1$ corresponds to Viña del Mar, the city with the most inhabitants (332,875) according to the 2017 Census [37]. According to the census, 402 out of 433 settlements had exposed inhabited buildings in the exposed areas.

Table 1. Fields used in the inventory for each coastal settlement and its application to the city of Arica. In ARClim, data for all coastal settlements can be downloaded by clicking the button Exportar datos", at the top right corner of the site https://arclim.mma.gob.cl/atlas/view/asentamien\T1\textquotedblrighttos_costeros/ (accessed on 12 October 2022).

Field	Description	Example
ID		ID001
Fishing cove	Name	Arica
Latitude	In degrees	−18.47402
Longitude	In degrees	−70.321417
Municipality	Name	Arica
Region	Name	Arica y Parinacota
Category	City/Town/Village/Hamlet	City
Type	Urban/Rural	Urban
Area	In km^2	43.51
Population	In inhabitants	202,131
Houses	In units	65,888

2.2.3. Sensitivity

The sensitivity index (S^{FL}) was defined as

$$S^{FL} = (C + B + P + H + F)/5, \qquad 0 < S \leq 1, \tag{4}$$

which equally weights the type of settlement (urban/rural), exposed buildings, population density, housing density, and fraction of inhabitants per housing. As all of these variables are of different nature, they were subjected to nondimensionalization and scaled between 0 and 1 to allow comparison. The weighting of these coefficients was equally set to 1/5, although they could be set according to expert judgement, local needs, or disciplinary criteria. The parameter C represents the type of settlement and is higher for rural or isolated sites (Table 2).

Table 2. Definition of category and type of coastal settlement, adapted from [37]. The parameter C weights the type of settlement in the sensitivity index given by Equation (4).

Category	C	Type	Inhabitants	Conditions
City	0.00	Urban	>5000	-
			1001–5000	Regional or provincial capital
Town	0.25	Urban	2001–5000	-
			1001–2000	Less than 50% of workforce develop primary activities
Village	0.50	Rural	301–2000	-
			1001–2000	Less than 50% of workforce develop primary activities
Hamlet	1.00	Rural	<301	-

The parameter B represents the exposed buildings defined as $B = 1$ if there are houses below 10 masl within the settlement and $B = 0$ if not. This parameter was computed using the exposed area data described in the previous section. The parameters P and H represent the relative population density and relative housing density, defined as

$$P = p/\max\{p\} \text{ and } H = h/\max\{h\}, \qquad 0 < P, H \leq 1, \tag{5}$$

where the population density (p) is expressed in terms of the number of inhabitants per unit area, with the maximum values corresponding to Punta Lavapie (−37.152° S–73.574° W) at $\max\{p\} = 184$ inhabitants/ha. Conversely, (h) is the housing density in the number of houses per unit area, with Iloca (34.930° S−72.180° W) having the maximum density of $\max\{h\} = 132$ houses/ha.

$$F = f/\max\{f\}, \qquad 0 < F \leq 1, \tag{6}$$

where F represents the ratio between inhabitants per house (f) and the maximum value in the site database (Punta Arenas, −53.155° S–70.901° W).

2.2.4. Risk

Lastly, the flooding risk index of coastal settlements $\left(R^{FL}\right)$ was computed as the multiplication of the exposure, flooding hazard, and sensitivity indices:

$$R^{FL} = E^{FL} \times H^{FL} \times S^{FL}, \qquad 0 \leq R^{FL} \leq 1. \tag{7}$$

Quantitative indices of all the components of risk (E^{FL}, H^{FL}, S^{FL}, and R^{FL}) were then divided into a qualitative scale of five levels, and then displayed as very low (*muy baja/o*), low (*baja/o*), moderate (*moderada/o*), high (*alta/o*), and very high (*muy alta/o*). The scale was implemented in tailored color ranges to facilitate visual inspection.

2.3. Operational Downtime Risk of Fishing Coves

An inventory of 545 fishing coves was built from information described in [35]. Each cove was identified by its name, code, latitude, longitude, municipality, region, and type. Additionally, the total number of fishers per cove, number of gleaners, number of fin-fishers, number of vessels, number of vessels with length overall (LOA) between 12 and 18 m, and number of vessels with LOA below 12 m were included in the inventory. The existence of artificial shelter (e.g., breakwaters), natural shelter (e.g., bay or harbor), berthing facilities (e.g., pier or ramp), and territorial use rights for fishing programs (TURFs) were also reported. Table 3 summarizes the definition of each term and its application to Arica fishing cove, as an example. The complete inventory is available in the ARClim web platform as described in the table caption.

The inventory was used to compute the exposure and the sensitivity to operational downtime, defined herein as the total time that the users are unable to conduct activities (e.g., load or unload cargo, dive or collect algae) due to extreme swell conditions.

The risk analysis was restricted to 302 fishing coves directly exposed to swells from the Pacific Ocean, specifically from the northernmost Arica (18.474° S–70.321° W), to the southernmost San Pedro, Purranque (40.943° S–73.865° W), thus covering nearly 2500 km of coastline. The risk analysis excluded 243 sites located in the Chilean inland Sea as they are not exposed to ocean swells and, thus, not affected by the specific hazard analyzed herein (downtime in this region is related to local winds and locally generated short waves, which would require high-resolution atmospheric models and their coupling with wave models, respectively). However, exposure and sensitivity indices for these sites are included in the web-based database as they provide valuable information to decision makers. As a way to show how the data can be linked to direct impacts over artisanal fishery food provision, risk values for each fishing cove were linked to the overall official landing values for 2017 [38].

Table 3. Fields used in the inventory for each fishing cove, and their values for the example of Arica cove. Data for all fishing coves can be downloaded from ARClim by clicking the button "Exportar datos", at the top right corner of the site https://arclim.mma.gob.cl/atlas/view/caletas_pescadores/ (accessed on 12 October 2022).

Field	Description	Example
ID		ID001
Fishing cove	Name	Arica
Latitude	In degrees	−18.47402
Longitude	In degrees	−70.321417
Municipality	Name	Arica
Region	Name	Arica y Parinacota
Type	Urban/Rural	Urban
Nf	Number of total fishers	1664
Ng	Number of gleaners	320
Nff	Number of fin-fishers	1344
Nv	Number of vessels	221
NvM	Number of vessels with $12 \leq LOA \leq 18$	42
Nvm	Number of vessels with $LOA \leq 12$	179
	Existence of artificial shelter; yes (1)/no (0)	0
	Existence of natural shelter; yes (1)/no (0)	1
	Existence of berthing facilities; yes (1)/no (0)	0
	Existence of TURF; yes (1)/no (0)	0

2.3.1. Hazard

Changes in operational downtime between the historical period (1985–2004) and the projection (2026–2045) were computed by comparing exceedance probability curves of significant wave height (Hs) at each fishing cove with maximum operational thresholds for different activities (Figure 4a). Thresholds were defined from the outcomes of three focus groups and 12 unstructured interviews to fishers of El Quisco (33.393° S–71.695° W), Las Cruces (33.502° S–71.620° W), Maitencillo (32.649° S–71.442° W), Ventanas (32.711° S-71.499° W), Ancud (41.873° S–73.803° W), and Calbuco (41.762° S–73.135° W). The analysis of these surveys shows that thresholds are not universal, as they depend on the experience of fishers, their use of wave forecast tools for offshore wave conditions (e.g., www.buoyweather.com (accessed on 12 October 2022) and www.windguru.cz (accessed on 12 October 2022), and local conditions they consider when deciding whether or not to launch activities. We conservatively used a threshold of Hs = 2.0 m regardless of the type of activity, vessel type, and infrastructure (Figure 4a). Figure 4b shows the exceedance probability curves of Hs at each fishing cove and the operational thresholds of Hs = 2.0 m. Local wave conditions were estimated by transforming offshore wave conditions from six GCMs to each cove using Snell's Law and small-amplitude wave theory.

The hazard $\left(H^{OP}\right)$ was computed as the difference between the probability of downtime for the projection (Pp) and its historical value (Ph):

$$H^{OP} = Pp - Ph, \qquad 0 \leq H^{OP}. \tag{8}$$

In cases where the downtime is reduced in the projection with respect to the historical period, $Pp < Ph$, the hazard was assumed to be zero $H^{OP} = 0$, since, due to the scarcity of fisheries, the time that fishermen can conduct operations was assumed to be larger than the one needed to capture quotas.

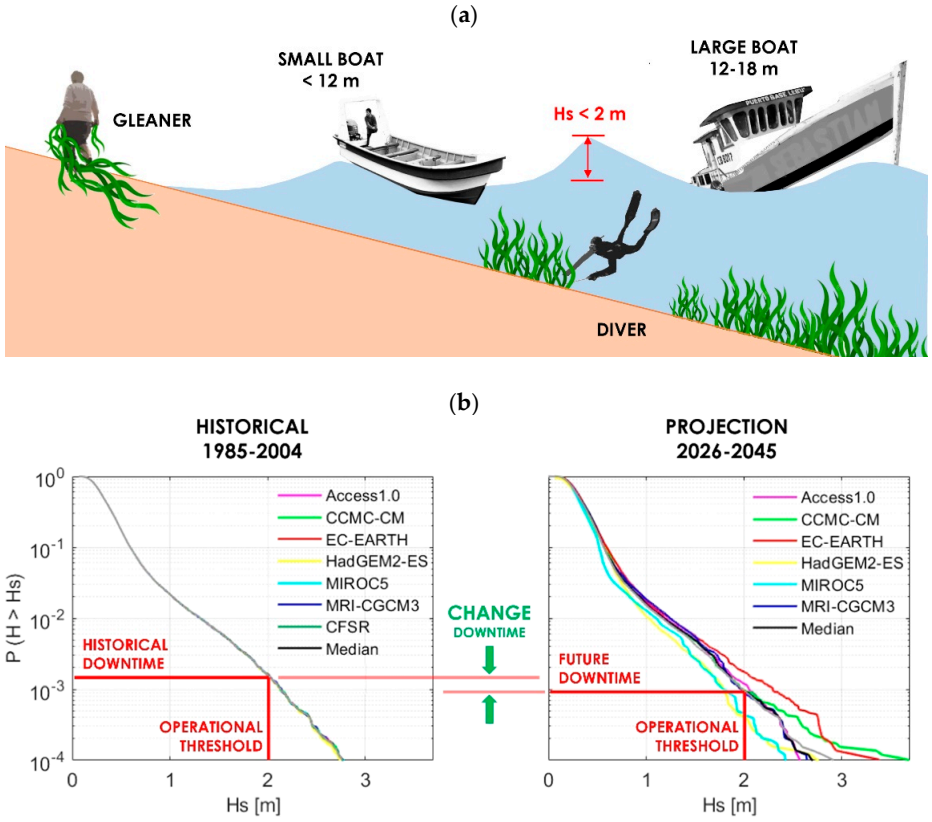

Figure 4. (**a**) Fishing activities analyzed in this study. (**b**) Computation of operational downtime in coves. Exceedance probability curves of unbiased values of significant wave height for the historical period (1985–2004) and mid-century (2026–2045) projection for six GCMs were used to compute the model median. The operational threshold of Hs = 2.0 m was used then to compute the historical and future downtime, the difference of which was used to compute the hazard. Note that, due to the application of the bias correction based on the Lemos et al. (2020) EGQM method, all curves collapsed into the benchmark (CFSR). For this specific example, downtime was reduced.

2.3.2. Exposure

The exposure (E^{OP}) was defined as the number of registered fishers (gleaners, divers, and fin-fishers) in each fishing cove, normalized by the number of registered fishermen in Lebu (4903) which has the highest population of all coves. Numerically, exposure was restricted to $0 < E^{OP} \leq 1$, where $E^{OP} = 1$ corresponds to Lebu.

2.3.3. Sensitivity

For each fishing cove, the sensitivity index (S^{OP}) was computed as a combination of the operational sensitivity index (So) and the structural sensitivity index (Se), according to the following equation:

$$S^{OP} = (So + Se)/2, \qquad 0 \leq S, So, Se \leq 1. \tag{9}$$

The values of all indices ranged between 0 (fully sensitive) and 1 (not sensitive). The operational sensitivity index weights the type of activity of registered fishers (gleaners, divers, or fin-fishers) and the type of vessel used with the following expression:

$$So = (Fn + Fe)/2. \tag{10}$$

The parameter Fn is the fraction of fishers which sail (e.g., total fishers minus gleaners), $Fn = (\ Np - Nr)/Np$. It is, thus, assumed that the fishing cove is more sensitive when more fishermen sail or dive, as they are more affected than gleaners by port closures.

Conversely, Fe is the fraction of minor boats with $LOA \leq 12$ m (Nem) with respect to the total number of vessels on each fishing cove (Ne), e.g., $Fe = Nem/Ne$. We assume that the larger the percentage of small boats a fishing cove has, the more sensitive it is. This is because large boats usually have more powerful inboard engines than the less strong outboard motors that small boats are equipped with, providing the former with better sailing capacity.

The structural sensitivity index is defined as follows:

$$Se = (U + I + BI + NS + TU)/5. \tag{11}$$

As all these variables are of different nature, they were subjected to nondimensionalization and scaled between 0 and 1 to allow comparison. The parameter U represents the degree of urbanization of the site and has values of $U = 1$ for urban and $U = 0$ for rural settlements. It is, thus, assumed that an urban fishing cove is better equipped with services and rescue aids than an isolated one.

The parameter I indicates whether the site has adequate infrastructure to provide artificial shelter to improve navigation. Values of $I = 1$ are assigned if the site has breakwater and $I = 0$ if not.

The parameter BI indicates whether the site has adequate berthing infrastructure to support the fishing activities. We assign values of $BI = 1$ if the site has infrastructure (e.g., piers or ramps), and $BI = 0$ if boats are pulled onto the beach with the aid of tractors or horses, or by the fishermen.

The parameter NS specifies if the site has natural shelter to winds and waves. We assume $NS = 1$ if the site is sited on a bay, protected by a peninsula, or located in a river outlet, and $NS = 0$ if it is open to the ocean.

The parameter TU indicates if the site has a fisher's union with territorial use rights for fishing programs, TURFs (Área de Manejo y Explotación de Recursos Bentónicos, AMERB). We assume that a fishing cove associated with a TURF has better organizational abilities and is, thus, less sensitive $(TU = 1)$ than a site which is not $(TU = 0)$.

2.3.4. Risk

The operational downtime risk index of fishing coves $\left(R^{OP}\right)$ was computed as the multiplication of the exposure, hazard, and sensitivity indices:

$$R^{OP} = E^{OP} \times H^{OP} \times S^{OP}, \qquad 0 \leq R^{OP} \leq 1. \tag{12}$$

Following the same standardized scheme in ARClim, quantitative indices of all the components of risk (R^{OP}, E^{OP}, H^{OP}, and S^{OP}) were divided into five quintiles and then displayed on a qualitative scale of five levels: very low, low, moderate, high, and very high.

3. Results

3.1. Flooding Risk of Coastal Settlements

Figure 5 shows the historical (Z_h) and projected flooding hazard (Z_p), computed from the superposition of the maximum yearly astronomical tide, storm surge, wave setup, wave swash, and sea-level rise. We can note that mean sea level (SLR) rise is the main contribution to the increase in flood level. Projected values of the contributions of storm surge (SS_p) and waves (i.e., the wave setup S_p and the swash R_p, which summed up lead to the wave runup W_p, according to [36]) have negligible differences with respect to the historical period. Lastly, the tide (T) is assumed to be the same for both periods, thus having no impact on the change in downtime. The increased flooding level and, thus, the hazard are evenly distributed in the study area. The computation of the flooded areas is available in cartographic maps in [17].

Figure 6 show the values of the hazard, exposure, sensitivity, and risk of coastal settlements to coastal flooding based on the graphical displays available in the ARClim web platform, using the qualitative color scale.

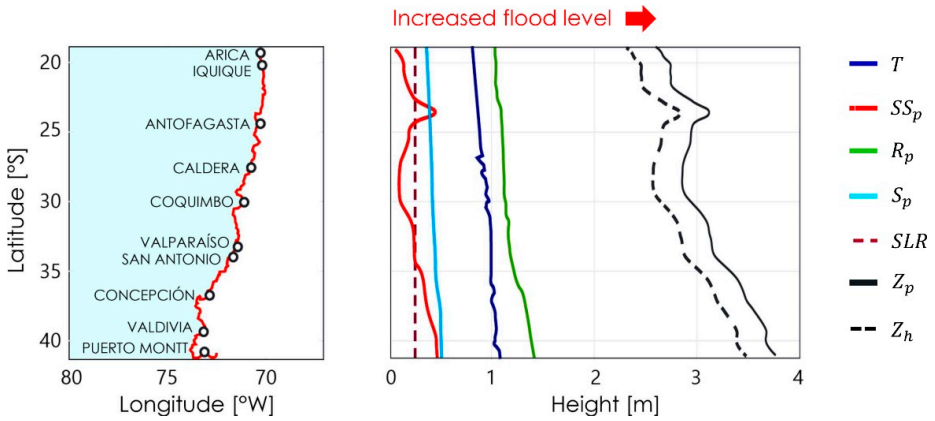

Figure 5. Estimation of the projected flooding hazard (Z_p) for the RCP 8.5 scenario in the period 2026–2045, computed from the superposition of the maximum yearly astronomical tide (T), storm surge (SS_p), wave setup (S_p), wave runup (R_p), wave swash (S_p), and sea-level rise (SLR). The flooding hazard for the historical period 1985–2004 (Z_h) is included. The data are computed at 0.1° intervals along the coastal region between Arica and Puerto Montt, where all 256 exposed settlements were located. The places shown in the rightmost figure are for reference only.

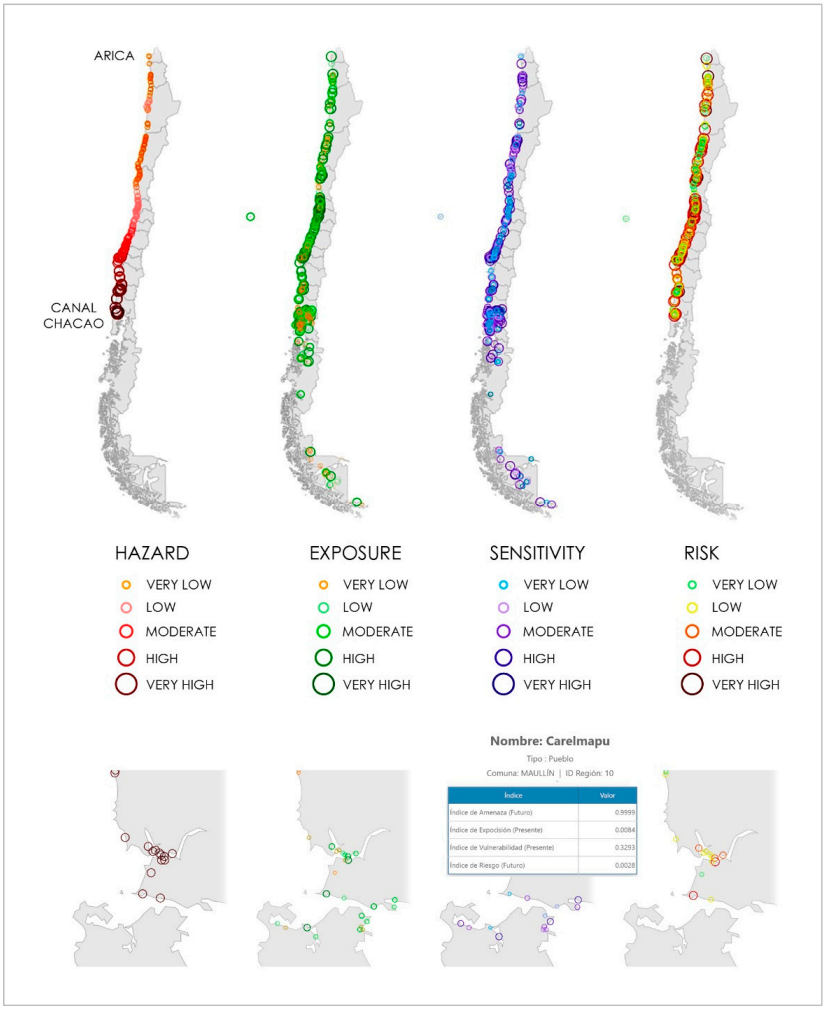

Figure 6. Relative values of the hazard, exposure, sensitivity, and risk of coastal settlements to coastal flooding. Bottom: Zoomed-in view covering Canal Chacao, including indices at Carelmapu (41.745° S–73.705° W). Available at https://arclim.mma.gob.cl/atlas/view/asentamientos_costeros/ (accessed on 12 October 2022).

The hazard gradually increases to the south due to subtle changes in the relative flood level. However, the exposure, sensitivity, and consequently, the risk are responsive to the highly variable latitudinal distribution of the country's coastal population. The northern desert is characterized by sparsely inhabited regions with low risk, interceded by larger coastal cities historically linked to trade with neighboring countries and mining. The central region is characterized by the metropolitan areas of Valparaíso and Concepción, having around one million inhabitants each. This region is associated with the highest values of risk throughout the country. To the south, the coast is sparsely inhabited, due to its complex geomorphology, limited connectivity, and harsh climate.

The ARClim data can provide particularly useful insights into the exposure of coastal settlements if lumped into national or regional information. For example, analysis shows that, nationwide, 589 census blocks and 18,338 buildings are located above the historical flood level but would be exposed to flooding in the projection, and 46,357 inhabitants were registered in such regions according to the last census. The dataset can also be aggregated on a regional level, as shown in Figure 7.

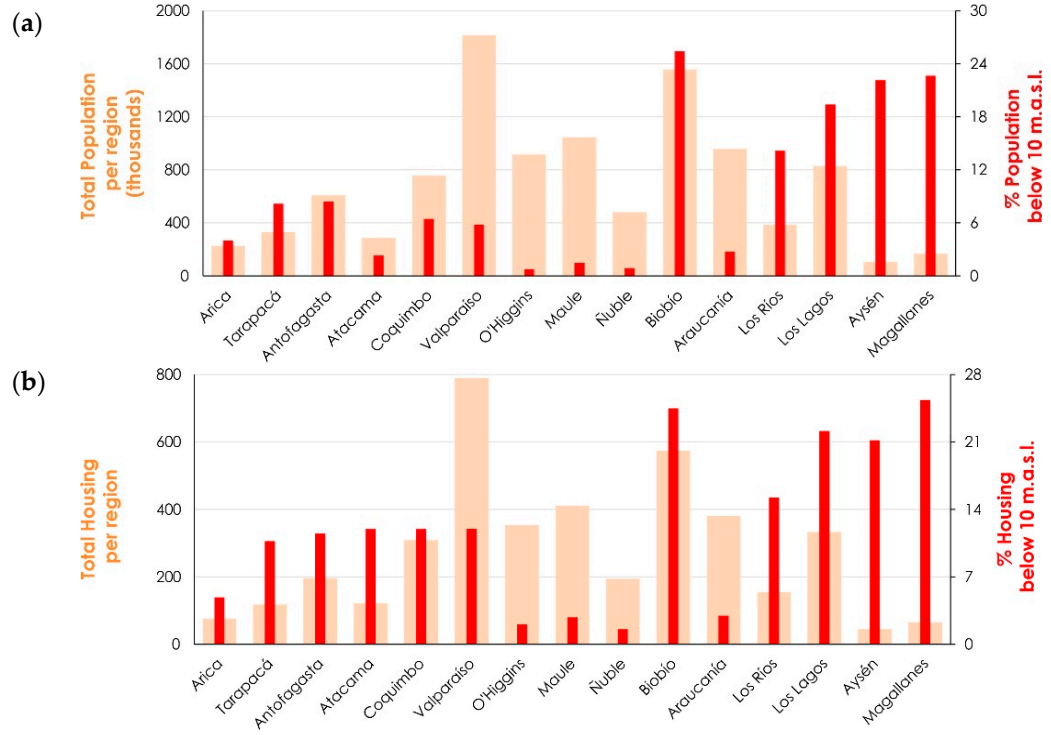

Figure 7. Examples of data aggregation for (**a**) population and (**b**) housing on a regional level. Shaded thick bars depict the total values of population and housing on each region, respectively. Red thin bars represent the percentages of population and housing on each region, respectively. The horizontal axis shows Chile's main administrative regions (from north to south).

3.2. Operational Downtime Risk of Fishing Coves

Table 4 shows the exceedance probability and the corresponding downtime (in h/year) associated with the threshold of $Hs = 2.0$ m for the historical period (1985–2004) and for the projection (2026–2045), averaged in 2° latitude bins in the coastal region exposed to ocean swells.

Figure 8 shows the display of the relative values of the hazard, exposure, sensitivity, and risk of fishing coves to operational downtime. Both in the figure and in Table 3, the hazard shows a clear pattern, where the northern and southernmost coves of the analysis show "very low" values, while central Chile from Caleta Carrizal Bajo-Huasco (28°4′47.4″ S–71°8′58.4″ W) to Caleta Cahuil-Pichilemu (34°28′46.77″ S–72°1′3.68″ W) show very high values. Thus, hazard is concentrated in the center–north of the country.

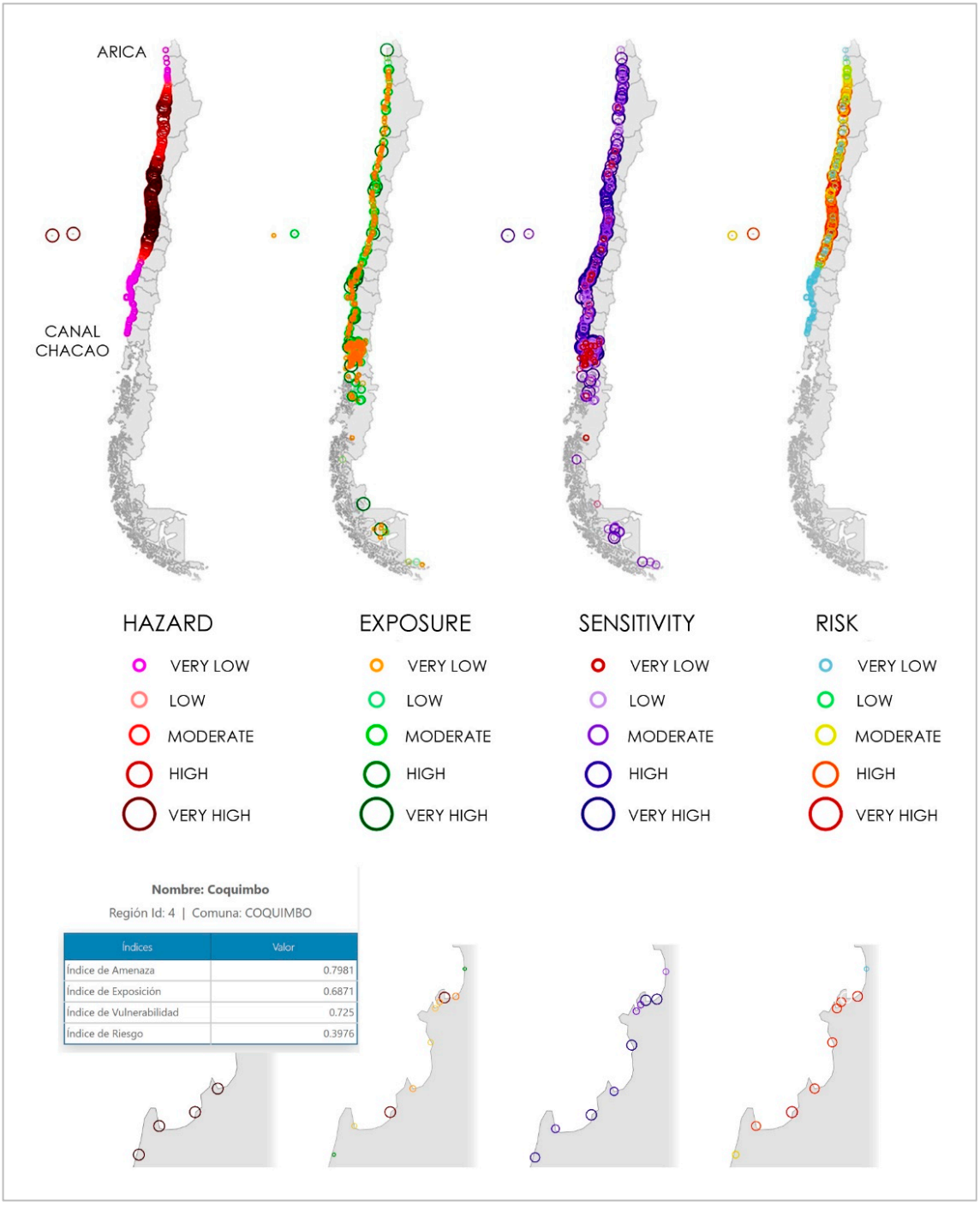

Figure 8. Top: Relative values of the hazard, exposure, sensitivity, and risk of fishing coves. Bottom: Zoomed-in view covering Coquimbo Bay and surroundings, including indices at Coquimbo fishing cove (36.530° W–72.959° W). Available at https://arclim.mma.gob.cl/atlas/view/caletas_pescadores/ (accessed on 12 October 2022).

Additional analysis of the fishing cove risk values can provide important information on the downtime risk for specific types of artisanal fisheries. Figure 9 shows the risk distributions for different types of fishery landings in 2017. The risk distribution varies significantly depending on the resource type. For instance, fin fish and giant squid are landed mainly from fishing coves with high risk factors, while algae, benthic resources, and rocky reef fish have a more heterogeneous risk distribution.

Table 4. Exceedance probability and downtime (in h/year) associated with a threshold of $Hs = 2.0$ m for the historical period (1985–2004) and for the projection (2026–2045), lumped every 2° of latitude in regions exposed to ocean swells.

	P (%)			Downtime (h/Year)		
	1985–2004	2026–2045	Change	1985–2004	2026–2045	Change
Latitude (° S)	*Ph* (%)	*Pp* (%)	*H*	*Dh*	*Dp*	*ΔD*
19	3.49	3.42	−0.07	306	300	−6
21	4.82	5.08	0.26	422	445	23
23	8.99	9.82	0.83	788	860	73
25	11.46	12.19	0.73	1004	1068	64
27	22.15	22.7	0.55	1940	1989	48
29	21.26	22.28	1.02	1862	1952	89
31	28.65	29.43	0.78	2510	2578	68
33	37.91	39.05	1.14	3321	3421	100
35	43.77	44.4	0.63	3834	3889	55
37	55.5	55.19	−0.31	4862	4835	−27
39	59.11	58.61	−0.50	5178	5134	−44
41	71.33	70.89	−0.44	6249	6210	−39

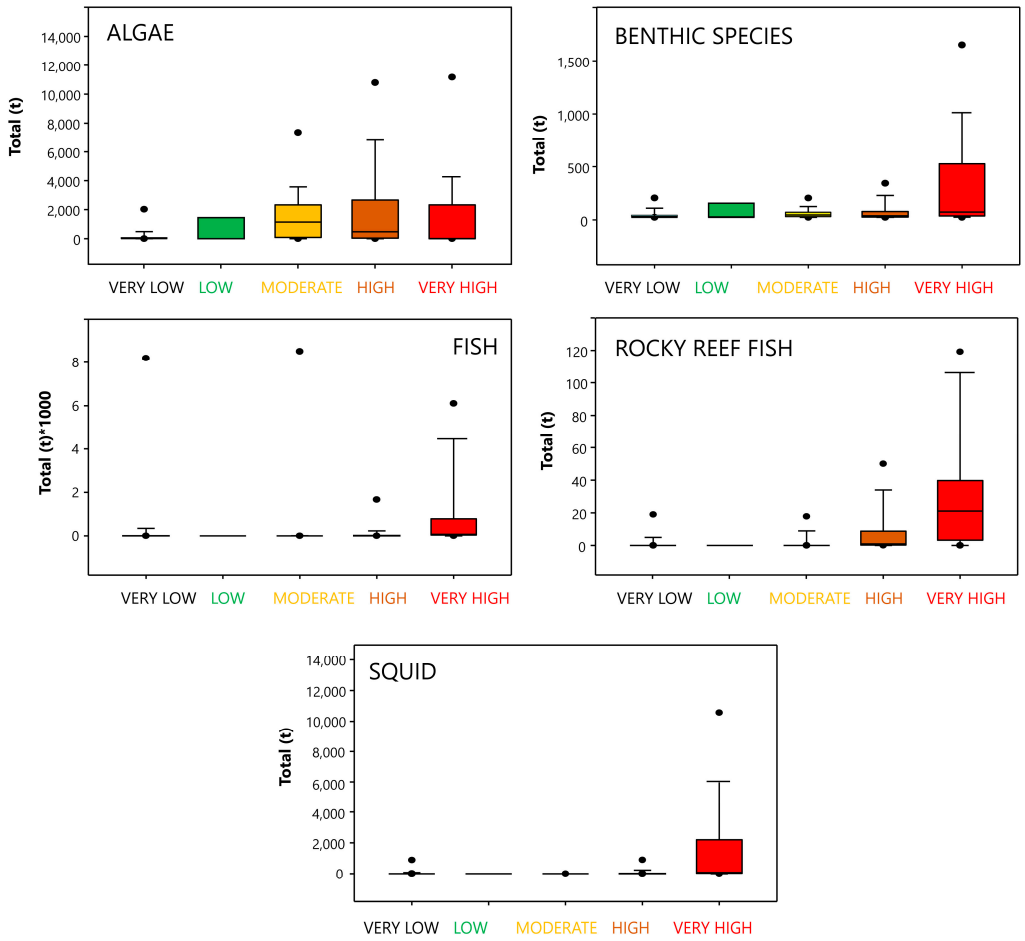

Figure 9. Fishery landings associated with fishing coves experiencing different levels of risk (very low, low, moderate, high, and very high) in the year 2017. Dots represent outliers, whiskers enclose 95% of the data, the interquartile range is depicted in colored bars and the median is shown with a black line.

4. Discussion

Below, we discuss some caveats and opportunities for improvement for the two cases that were presented in this study.

4.1. Flooding Risk of Coastal Settlements

Our approach in the risk assessment has pitfalls in the estimation of the hazard, exposure, and sensitivity, which could be addressed in future studies. Regarding the hazard, the flood level used to compute the risk in coastal settlements was calculated by summing a deterministic measure of the astronomical tide [34], statistical values of storm surge available in [33], and those computed from various GCM (waves and SLR) for both the historical period and the projection, taking no account of the temporal sequence of each variable nor the local effects that nearshore waves experience due to an irregular seafloor. Additionally, data characterizing storm surge and tides did not strictly coincide with the analyzed periods. Fortunately, tide is bounded, periodic, and relatively constant; thus, using one particular year is a reasonable approximation to characterize this variable. Storm surge, however, is climate-dependent. The reason to use data from 2010 for the historical period and 2040 for the projection was based on the practical reason that it was readily available during the project. As storm surge was the least important contribution to flood level, we believe that using these data should not have a relevant impact on the results. Estimation of the hazard could be improved by computing the flood level for each sea state (1–3 h depending on the availability of data) and estimating this quantity for different return periods on the basis of an extreme value analysis. Local estimates of wave climate could be obtained using an extended version of Massel's spectral method ([39], Equation (6)), by adding processes to the original expression for refraction and shoaling. These options were not addressed in the present study as (a) homogeneous time series for storm surge were unavailable at the time ARClim was built, and (b) the computational costs of modeling local wave conditions at 256 coastal settlements, most of which have no detailed bathymetry, was beyond the reach of the project.

A major limitation of the computation of the exposure deals with the heterogeneity of the different topographic datasets from which the exposure was computed. As mentioned, the area below 10 masl was computed from three different satellite datasets and 52 topographic surveys covering only a few of the coastal settlements. The variability among the three sources of satellite data proved to be significant throughout the country, as shown in the example of Figure 2a. Additionally, the difference between exposed areas computed from satellite datasets and topographic surveys was found to be significant in the few sites where the survey data were available as seen in the examples of Figure 2b,c for Coquimbo Bay. The computation of relative risk, therefore, is highly dependent on the topographic sources used at each site.

A second limitation to the exposure assessment deals with the assumption that the topography and, thus, the exposure remains constant between the historical period and the projection. Estimates of coastal flooding are sensitive to the vertical position of the coast, which is shaped by the subduction of the Nazca Plate beneath South America [40]. The region has been affected by several megathrust earthquakes, such as the M9.5 1960 Valdivia earthquake [41], which produced vertical changes of +5.7 m to −2.7 m in the coastline, or the M8.8 2010 Maule earthquake, where a maximum uplift of +3.44 m was measured [42]. Although these values are comparable to centuries of climate-driven SLR, their relatively low probability of occurrence [43] makes their occurrence within the analyzed projection (2026–2045) minor, but not negligible. For example, the authors of [16] used a dataset of 25 measures of co-seismic land changes in the vicinity of the state-owned Chilean ports to analyze their influence in overtopping discharge. They concluded that co-seismic subsidence could notably increase overtopping compared to the no-earthquake scenario, while co-seismic uplift would counterbalance changes in wave climate and SLR, yielding a reduction in overtopping. Similarly, the authors of [44] provided a dataset of 90 measures of co-seismic uplift or subsidence for historical earthquakes in the vicinity of 45 beaches,

80% of which have experienced erosion in the last decades. They, however, did not correlate the actual values of deformation with rates of shoreline retreat, and just mentioned them as a possible source of coastal erosion.

Regarding the risk calculations themselves, sensitivity, exposure, and risk were computed with weighting coefficients that were defined by the authors in the present approach. However, the definition of such coefficients could be set according to expert judgement, local needs, or disciplinary criteria defined with the involvement of potential users, policy makers, and stakeholders.

We also note that the municipal scale of many of the variables included in the analysis is insufficient to resolve local effects, which could be evaluated with a local definition of the hazard, a disaggregated analysis of the exposure for individual buildings or census blocks, and techniques such as fragility curves, to compute an absolute and quantitative value of the risk.

Lastly, the standardized display ARClim uses to present the components of risk on a qualitative scale of five levels allows only a comparative risk assessment which may be useful for users on a local, regional, or national level, but insufficient for specific users which may be interested in calculating the costs of inaction or adaptation schemes. The present approach, however, is useful to identify priorities among municipalities and sectors which could be further analyzed with more detailed studies. The analysis of the flooding hazard at coastal settlements could be complemented under a multi-risk analysis using other ARClim indices associated with beach erosion, urban flooding, and riverine floods (links to these indices are available in the Data Availability Statement).

4.2. Operational Downtime Risk of Fishing Coves

The risk assessment of climate-driven impact on fishing coves also has room for improvement. The hazard estimate could be improved with better estimates of local wave climate in those few sites where highly detailed bathymetry is available, following the procedure used in [16] for seven state-owned ports throughout the country.

Changes in downtime were computed using operational thresholds based on the local significant wave height, with no consideration of other physical variables that determine the boat's maneuver (e.g., wave period and direction, winds, currents, the presence of breakwaters, or sand shallows), its load distribution, the pilot's knowledge, local traditions, and the judgement of the maritime authority, which ultimately decrees port shutdowns. Additionally, the computation assumes that the thresholds will remain constant regardless of technological improvements aiding the boats (e.g., better propulsion systems), local meteorological forecasts and in situ records, or improvements in shelter (e.g., construction of breakwaters and dredging of navigation channels).

Another improvement deals with the estimation of local wave conditions at each site. This simplified computation of downtime, based on Snell's law and the small-amplitude wave theory, could be improved using a combination of phase-resolving wave models that capture local phenomena (e.g., diffraction and reflection) and spectral wave transformation on the basis of the superposition of elementary spectral components [39]. This, however, could be improved in a relatively small portion of fishing coves where bathymetric data are available [45].

Results of this study suggest that the analysis of the operational dimension associated with fishing port shutdowns at coves can be easily complemented with landing values as a way to begin estimating potential losses in fisheries. Future studies could assess the economic value associated with the increased downtime at each cove using avoided/induced cost methods, resulting in estimates of tons that would be lost because of the increased downtime and their valuation. These could also use different operational threshold values.

4.3. Broader Aspects of ARClim

ARClim includes risk analyses for multiple social, environmental, and productive sectors encompassing the whole country. While, in this work, we focused on some of

the risks due to climate change along the Chilean coast, some of the lessons are generally applicable to other impact chains, as a common framework was used in the ARClim development. First and foremost is the limitation imposed using present-day estimates of exposure and sensitivity. We do know that both features are continually changing due to demographic trends, technological advances, and social movements. Nonetheless, quantifying exposure and sensitivity was a major challenge even when using the data currently available; their future changes seem even more complicated to address. Future efforts need to incorporate, at the very least, model-based demographic projections that, within a horizon of a few decades, are as robust as climate projections. Changes in the way the people distribute across the territory are more complicated, setting aside changes in social development and technological innovation, but consideration of a few realistic scenarios (as much as we do with climate scenarios) may be a way to tackle this problem. Thus, a more realistic appraisal of risk is needed to realize that exposure and sensitivity change, perhaps, even more rapidly than climate. This is a pressing issue, since, as we found in the coastal zone, the heterogeneous distribution of the risk comes largely from the spatial variability in exposure and sensitivity.

A second issue that emerges from the present study is that, for definition, we assessed the risk associated with specific activities (e.g., operational downtime of fishing). The maps presented in ARClim (e.g., Figures 6 and 8) can certainly support the prioritization of specific adaptation measurements for this activity. They inform the national authorities where the risk is largest and lowest. However, local authorities and citizens depend on multiple activities carried out in the same place (and sometimes by the same people). Let us consider a simple case in which a coastal town depends on artisanal fishing and tourism; suppose that the first activity has a low risk, and the second has a high risk. Recall that ARClim provides quantitative measurements of the relative (to the rest of the towns and coves) risk for a given activity. The outstanding question is then how this multi-sectorial information can be merged to generate an aggregated risk index useful for the local community.

Lastly, the relative risk presented in ARClim is assessed according to units of territory (towns, coves, ports, cities, and municipalities) regardless of the risk elsewhere and the risk of other activities. However, if risk begins to materialize in each spatial unit, it is likely that people will be displaced within the region (and even among regions) or change their main activity, thus affecting the overall risk of the region. Once again, integration of risk among space and sectors remains as a big challenge for future versions of ARClim.

The issues outlined above do not undermine the results presented in ARClim on which this work is founded. In contrast, the sectorial and geographically explicit assessment of the relative risk that ARClim produced is a necessary building block upon which a more comprehensive and integrated regional or even national risk assessment can be constructed.

5. Conclusions

Operational tools such as ARClim provide the basis for an improved understanding of climate change that can underpin improved management of coastal zones. Specifically, ARClim provides decision makers and stakeholders with a tool to visualize comparative estimates of hazards, exposure, and sensitivity, which may enable them to prioritize actions in units with relatively high risk within one sector. Because of the standardized nature of the ARClim framework, this approach additionally allows direct and fine-scale comparisons among different systems. This approach and its future iterations are likely to be applicable in a variety of other countries facing similar challenges. As shown in the two highlighted applications for coastal zones, it allows users understand the heterogeneity of climate-related risks, as such information provides a scientific basis for long-term planning and may lead to more targeted policy and management interventions. By operationalizing key features of hazards, exposure, sensitivity, and risk in spatial terms, ARClim can be a valuable, integrative tool. This is especially true considering that much of the data in the

ARClim platform were previously unavailable to the public. As with any decision support tool, ARClim should be constantly updated and improved.

Author Contributions: Conceptualization, P.W., M.C.-L., R.G. and F.M.; methodology, P.W., M.C.-L. and S.G.; software, M.F.; formal analysis, P.W. and M.C.-L.; data curation, J.M., C.E. and C.L.; draft preparation, P.W.; review and editing, S.G., M.F., R.G. and C.L.; visualization, M.F.; project administration, R.G. and F.M.; funding acquisition, R.G. and F.M. All authors have read and agreed to the published version of the manuscript.

Funding: ARClim was funded by German agency GIZ via grant 81246394.

Informed Consent Statement: Not applicable.

Data Availability Statement: ARClim is available at https://arclim.mma.gob.cl/ (accessed on 12 October 2022). Specific results for flooding of coastal settlements can be found at https://arclim.mma.gob.cl/atlas/view/asentamientos_costeros/ (accessed on 12 October 2022) for operational downtime and at https://arclim.mma.gob.cl/atlas/view/caletas_pescadores/ (accessed on 12 October 2022) for fishing coves. Other related links are beach erosion (https://arclim.mma.gob.cl/atlas/view/playas/, accessed on 12 October 2022), urban flooding (https://arclim.mma.gob.cl/atlas/view/inundaciones_urbanas/, accessed on 12 October 2022), and riverine floods (https://arclim.mma.gob.cl/atlas/view/desbordes_rios/, accessed on 12 October 2022).

Acknowledgments: ARClim is a project by the Chilean Ministry of Environment. It was developed by Centro de Ciencia del Clima y la Resiliencia (CR2) ANID/FONDAP/15110009 and Centro de Cambio Global (CCG) with the aid of other national and international institutions. The authors acknowledge the support of SECOS Iniciativa Cientifica Milenio ICN2019_015 and ANID PIA/BASAL FB 0002 and the Research Center for Integrated Disaster Risk Management (CIGIDEN), ANID/FONDAP/15110017.

Conflicts of Interest: The authors declare no conflict of interest.

References

1. MMA. Framework Law on Climate Change (Law 21,455) Was Enacted in Chile. Available online: https://www.bcn.cl/leychile/navegar?idNorma=1177286 (accessed on 12 October 2022).
2. Pica-Téllez, A.; Garreaud, R.; Meza, F.; Bustos, S.; Falvey, M.; Ibarra, M.; Duarte, K.; Ormazábal, R.; Dittborn, R.; Silva, I. *Informe Proyecto ARClim: Atlas de Riesgos Climáticos para Chile*; Centro de Ciencia del Clima y la Resiliencia, Centro de Cambio Global UC and Meteodata for the Ministerio del Medio Ambiente via La Deutsche Gesellschaft für Internationale Zusammenarbeit (GIZ): Santiago, Chile, 2020.
3. GIZ; EURAC. Risk Supplement to the Vulnerability Sourcebook. In *Guidance on How to Apply the Vulnerability Sourcebook's Approach with the New IPCC AR5 Concept of Climate Risk*; GIZ: Bonn, Germany, 2017.
4. IPCC. Annex II: Glossary [Möller, V.R., et al. (eds.)]. In *Climate Change 2022: Impacts, Adaptation and Vulnerability. Contribution of Working Group II to the Sixth Assessment Report of the Intergovernmental Panel on Climate Change*; Pörtner, H.-O., Roberts, D.C., Adams, H., Eds.; Cambridge University Press: Cambridge, UK; New York, NY, USA, 2022; pp. 2897–2930. [CrossRef]
5. IPCC. *Climate Change 2014: Impacts, Adaptation, and Vulnerability. Part A: Global and Sectoral Aspects. Contribution of Working Group II to the Fifth Assessment Report of the Intergovernmental Panel on Climate Change*; Cambridge University Press: Cambridge, UK; New York, NY, USA, 2014. Available online: http://www.ipcc.ch/report/ar5/wg2/ (accessed on 12 October 2022).
6. Boisier, J.P.; Alvarez-Garreton, C.; Cordero, R.; Damian, A.; Gallardo, L.; Garreaud, R.; Lambert, F.; Ramallo, C.; Rojas, M.; Rondanelli, R. Anthropogenic drying in central-southern Chile evidenced by long term observations and climate model simulations. *Elem. Sci. Anth.* **2018**, *6*, 74. [CrossRef]
7. Winckler, P.; Aguirre, C.; Farías, L.; Contreras-López, M.; Masotti, I. Evidence of climate-driven changes on atmospheric, hydrological, and oceanographic variables along the Chilean coastal zone. *Clim. Chang.* **2020**, *163*, 633–652. [CrossRef]
8. Arns, A.; Dangendorf, S.; Jensen, J.; Talke, S.; Bender, J.; Pattiaratchi, C. Sea-level Rise Induced Amplification of Coastal Protection Design Heights. *Sci. Rep.* **2017**, *7*, 40171. [CrossRef] [PubMed]
9. Hall, J.W.; Sayers, P.B.; Dawson, R.J. National-scale assessment of current and future flood risk in England and Wales. *Nat. Hazards* **2005**, *36*, 147–164. [CrossRef]
10. Mokrech, M.; Nicholls, R.J.; Richards, J.A.; Henriques, C.; Holman, I.P.; Shackley, S. Regional impact assessment of flooding under future climate and socio-economic scenarios for East Anglia and North West England. *Clim. Chang.* **2008**, *90*, 31–55. [CrossRef]
11. Heberger, M.; Cooley, H.; Herrera, P.; Gleick, P.H.; Moore, E. Potential impacts of increased coastal flooding in California due to sea-level rise. *Clim. Chang.* **2011**, *109*, 229–249. [CrossRef]
12. Toimil, A.; Losada, I.J.; Díaz-Simal, P.; Izaguirre, C.; Camus, P. Multi-sectoral, high-resolution assessment of climate change consequences of coastal flooding. *Clim. Chang.* **2017**, *145*, 431–444. [CrossRef]

13. Winckler, P.; Contreras-López, M.; Campos-Caba, R.; Beyá, J.; Molina, M. El temporal del 8 de agosto de 2015 en las regiones de Valparaíso y Coquimbo, Chile Central. *Lat. Am. J. Aquat.* **2017**, *45*, 622–648. [CrossRef]
14. Carvajal, M.; Contreras-López, M.; Winckler, P.; Sepúlveda, I. Meteotsunamis Occurring Along the Southwest Coast of South America During an Intense Storm. *Pure Appl. Geophys.* **2017**, *174*, 3313–3323. [CrossRef]
15. McGranahan, G.; Balk, D.; Anderson, B. The rising tide: Assessing the risks of climate change and human settlements in low elevation coastal zones. *Environ. Urban* **2007**, *19*, 17–37. [CrossRef]
16. Winckler, P.; Esparza, C.; Mora, J.; Melo, O.; Bambach, N.; Contreras-López, M.; Sactic, M.I. Impacts in ports on a tectonically active coast for climate-driven projections under the RCP 8.5 scenario: 7 chilean ports under scrutiny. *Coast. Eng.* **2022**, *64*, 387–405. [CrossRef]
17. MMA. Volumen 7 Vulnerabilidad y Riesgo en Caletas Pesqueras. In *Determinación del Riesgo de los Impactos del Cambio Climático en las Costas de Chile*; Ministerio del Medio Ambiente: Santiago, Chile, 2019.
18. Harley, M. Coastal Strom Definition. In *Coastal Storms: Processes and Impacts*; Ciavola, P., Coco, G., Eds.; John Wiley and P. Sons.: New York, NY, USA, 2017; pp. 1–19. ISBN 978-1-118-93710-5.
19. Carvajal, M.; Winckler, P.; Garreaud, R.; Igualt, F.; Contreras-López, M.; Averil, P.; Cisternas, M.; Gubler, A.; Breuer, W. Extreme sea levels in Rapa Nui (Easter Island) during intense Atmospheric Rivers. *Nat. Hazards* **2021**, *106*, 1619–1637. [CrossRef]
20. Camus, P.; Losada, I.; Izaguirre, C.; Espejo, A.; Menéndez, M.; Pérez, J. Statistical Wave Climate Projections for Coastal Impact Assessments. *Earth's Future* **2017**, *5*, 918–933. [CrossRef]
21. Izaguirre, C.; Losada, I.J.; Camus, P.; Vigh, J.L.; Stenek, V. Climate Change Risk to Global Port Operations. *Nat. Clim. Chang.* **2021**, *11*, 14–21. [CrossRef]
22. Tolman, H. *User Manual and System Documentation of WAVEWATCH III R Version 4.18*; Technical Note; Environmental Modeling Center, Marine Modeling and Analysis Branch: Washington, DC, USA, 2014.
23. Taylor, K.E.; Stouffer, R.J.; Meehl, G.A. An Overview of CMIP5 and the Experiment Design. *Bull. Am. Meteorol. Soc.* **2012**, *93*, 485–498. [CrossRef]
24. Church, J.; Clark, P.; Cazenave, A.; Gregory, J.; Jevrejeva, S.; Merrifield, M.; Milne, G.A.; Nerem, R.S.; Nunn, P.D.; Payne, A.J.; et al. *Sea Level Change, Climate Change 2013: The Physical Science Basis, in Contribution of Working Group I to the Fifth Assessment Report of the Intergovernmental Panel on Climate Change*; Cambridge University Press: New York, NY, USA, 2013; Volume 13, pp. 1137–1216. Available online: https://www.ipcc.ch/report/ar5/wg1/ (accessed on 12 October 2022).
25. Hemer, M.A.; Trenham, C.E. Evaluation of a CMIP5 Derived Dynamical Global Wind Wave Climate Model Ensemble. *Ocean Model.* **2016**, *103*, 190–203. [CrossRef]
26. NGDC. 2-minute Gridded Global Relief Data (ETOPO2) v2. National Geophysical Data Center, NOAA. Available online: https://www.ngdc.noaa.gov/mgg/global/etopo2.html (accessed on 14 March 2020). [CrossRef]
27. Wessel, P.; Smith, W.H. A Global, Self-consistent, Hierarchical, High-resolution Shoreline Database. *J. Geophys. Res. Solid Earth* **1996**, *101*, 8741–8743. [CrossRef]
28. Beya, J.; Álvarez, M.; Gallardo, A.; Hidalgo, H.; Winckler, P. Generation and Validation of the Chilean Wave Atlas Database. *Ocean Model.* **2017**, *116*, 16–32. Available online: https://oleaje.uv.cl/descargas.html (accessed on 12 October 2022). [CrossRef]
29. Lemos, G.; Menendez, M.; Semedo, A.; Camus, P.; Hemer, M.; Dobrynin, M.; Miranda, P.M. On the Need of Bias Correction Methods for Wave Climate Projections. *Glob. Planet Chang.* **2020**, *186*, 103109. [CrossRef]
30. Saha, S.; Moorthi, S.; Pan, H.-L.; Wu, X.; Wang, J.; Nadiga, S.; Tripp, P. The NCEP Climate Forecast System Reanalysis. *Bull. Am. Meteorol. Soc.* **2010**, *91*, 1015–1058. [CrossRef]
31. Integrated Climate Data Center; Hamburg University. THREDDS Data Server. Available online: https://icdc.cen.uni-hamburg.de/thredds/catalog/ftpthredds/ar5_sea_level_rise/catalog.html (accessed on 14 March 2020).
32. Slangen, A.B.A.; Carson, M.; Katsman, C.A.; Van de Wal, R.S.W.; Köhl, A.; Vermeersen, L.L.A.; Stammer, D. Projecting twenty-first century regional sea-level changes. *Clim. Chang.* **2014**, *124*, 317–332. [CrossRef]
33. CEPAL. Efectos del Cambio Climático en la costa de América Latina y el Caribe. Dinámicas, Tendencias y Variabilidad Climática. p. 265. Available online: https://www.cepal.org/es/publicaciones/3955-efectos-cambio-climatico-la-costa-america-latina-caribe-dinamicas-tendencias (accessed on 12 October 2022).
34. SHOA. Tablas de Marea de la Costa de Chile 2022. SHOA Pub. 3009. Available online: http://www.shoa.cl (accessed on 12 October 2022).
35. MMA. *Volumen 2: Exposición, en "Determinación del Riesgo de los Impactos del Cambio Climático en las costas de Chile"*; Ministerio del Medio Ambiente: Santiago, Chile, 2019.
36. Stockdon, H.F.; Holman, R.A.; Howd, P.A.; Sallenger, A.H., Jr. Empirical parameterization of setup, swash, and runup. *Coast. Eng.* **2006**, *53*, 573–588. [CrossRef]
37. INE. *Ciudades, Pueblos, Aldeas y Caseríos 2019*; Instituto Nacional de Estadística: Santiago de Chile, Chile, 2019.
38. SERNAPESCA. Desembarques Artesanales por Región, Caleta, Especie. 2017. Available online: www.sernapesca.cl (accessed on 12 October 2022).
39. Massel, S. *Ocean Surface Waves: Their Physics and Prediction*; Advanced Series on Ocean Engineering; World Scientific Publishing Company: Singapore, 1996; Volume 11, p. 491.
40. Giesecke, A.; Capera, A.G.; Leschiutta, I.; Migliorini, E.; Valverde, L.R. The CERESIS Earthquake Catalogue and Database of the Andean Region: Background, Characteristics and Examples of Use. *Ann. Geophys.* **2004**, *47*, 421–435. [CrossRef]

41. Plafker, G.; Savage, J.C. Mechanism of the Chilean Earthquakes of May 21 and 22, 1960. *Geol. Soc. Am. Bull.* **1970**, *81*, 1001–1030. [CrossRef]
42. Fritz, H.M.; Petroff, C.M.; Catalán, P.A.; Cienfuegos, R.; Winckler, P.; Kalligeris, N.; Synolakis, C.E. Field Survey of the 27 February 2010 Chile Tsunami. *Pure Appl. Geophys.* **2011**, *168*, 1989–2010. [CrossRef]
43. Poulos, A.; Monsalve, M.; Zamora, N.; de la Llera, J.C. An Updated Recurrence Model for Chilean Subduction Seismicity and Statistical Validation of Its Poisson Nature. *Bull. Seismol. Soc. Am.* **2019**, *109*, 66–74. [CrossRef]
44. Martínez, C.; Winckler, P.; Agredano, R.; Esparza, C.; Torres, I.; Contreras-López, M. Coastal erosion in sandy beaches along a tectonically active coast: The Chile study case. *Prog. Phys. Geogr. Earth Environ.* **2021**, *46*, 250–271. [CrossRef]
45. SHOA. Catálogo de Cartas y Publicaciones Náuticas. Pub. SHOA 3000. Available online: https://shoabucket.s3.amazonaws.com/shoa.cl/documentos/publicaciones/3000.pdf (accessed on 12 October 2022).